

# SCRAP MELTING IN BOF: INFLUENCE OF PARTICLE SURFACE AND SIZE DURING DYNAMIC CONVERTER MODELLING\*

Florian Markus Penz<sup>1</sup>  
Johannes Schenk<sup>2</sup>  
Philip Bundschuh<sup>3</sup>  
Harald Panhofer<sup>4</sup>  
Krzysztof Pastucha<sup>5</sup>  
Bernhard Maunz<sup>6</sup>

## Abstract

The increase in Basic Oxygen Furnace (BOF) plants in steelmaking has given rise to renewed interest in a dynamic simulation of the BOF process. Material and process costs can be saved with optimized process times and targeted charging of scrap and slag formers. Beside hot metal, scrap is the main source of iron in the BOF process. Furthermore, scrap is used as a coolant during the process due to exothermal chemical reactions occurring in the BOF. In this paper, the melting and dissolution behaviour of scrap in the BOF process is discussed. A new dynamic thermodynamic and kinetic Matlab® model used to simulate scrap melting behaviour as a function of various scrap surface parameters and particle size is presented, as well as the influence of scrap properties on liquid bath temperature and final crude steel composition after a defined blowing period.

**Keywords:** Scrap dissolution and melting; Thermodynamics; Kinetics; Dynamic BOF modelling.

<sup>1</sup> Dipl.-Ing., Researcher, K1-MET GmbH, Linz, Upper Austria, Austria.

<sup>2</sup> Univ.-Prof. Dipl.-Ing. Dr. techn., Professor, Chair of Ferrous Metallurgy, Montanuniversitaet Leoben, Leoben, Styria, Austria & CSO, K1-MET GmbH, Linz, Upper Austria, Austria.

<sup>3</sup> Dipl.-Ing. Dr.mont., University Assistant, Chair Ferrous Metallurgy, Montanuniversitaet Leoben, Leoben, Styria, Austria.

<sup>4</sup> Dipl.-Ing., Research Engineer, Research and Development Steelplant/ Technical Processes/ Business Unit Bramme, voestalpine Stahl GmbH, Linz, Upper Austria, Austria.

<sup>5</sup> Dipl.-Ing., Senior Expert, Stainless Steelmaking Converter Steelmaking, Primetals Technologies Austria GmbH, Linz, Upper Austria, Austria.

<sup>6</sup> Dipl.-Ing., Research Engineer, Research and Development, voestalpine Stahl Donawitz GmbH, Donawitz, Styria, Austria.

## 1 DESCRIPTION OF THE DYNAMIC BOF MODEL USED

The invention of the LD-converter in 1952 and 1953 in Linz and Donawitz, Austria, enables the conversion of hot metal into crude steel, in short blowing periods of around 20 minutes or less, resulting in increasing dominance of the BOF process in the steelmaking industry. Around 75 wt.-% to 95 wt.-% of metallic charge in the converter is hot metal. The remaining iron containing charge is steel scrap which is mainly used, due to exothermic oxidation reactions of carbon, silicon, manganese and phosphorus, as a coolant. The two main tasks of the BOF are decarburization and dephosphorization of the hot metal. Decarburization is done with technically pure oxygen. It is blown onto the liquid metal surface at supersonic velocity. This results in an ejection of metal droplets followed by an increase in the reaction surface and the oxidation of impurities. [1 - 4]

Classified as a single-zone model, based on thermodynamics and kinetic calculation, the BOF model described is coded in Matlab®. The single reaction zone in the converter process is assumed to be a heterogeneous thermodynamic system. All components except carbon can be conveyed along the interfacial surface between the slag and metal phases due to simultaneous chemical oxidation reactions to the slag phase. Carbon is oxidized to gaseous carbon monoxide, which is assumed to be removed instantaneously from the interfacial surface. Equilibrium thermodynamics of post combustion is neglected due to a non-reversible oxidation process. Blown oxygen and oxygen sucked from the atmosphere define the post combustion, the main influences being the lance position and the blowing rate. [4 - 7]

During the BOF process simulation the blowing oxygen consumption theory by V.E. Grum-Grzhimaylo for Bessemer converters is used instead of the chain reaction theory for metal burning. [8] It is assumed that only iron is oxidized by blown oxygen and the remaining elements in the liquid metal react further with the wustite formed. According to this assumption, the blown oxygen leads to a change in the chemical compositions of the metal and slag phases inside the thermodynamic system during the blowing period. Another impact of the melt and slag composition is given due to the simultaneous chemical reactions on the interfacial surface. Also the dissolution and melting behaviour of the charged materials has a strong influence. [5]

The concurrent oxidation-reduction reactions between metal and slag are explained by the coupled reaction model developed by Ohguchi et al. [9]. Japanese research studies commonly utilize this model for investigations of the influence of kinetic parameters on chemical reaction rates as well as dephosphorization and desulphurization processes. [9 - 16] Based on thermodynamic data, a system of simultaneous chemical reactions between the slag and metal phases occurs at the interface. The chemical equations were published by Y. Lytvynyuk et al. [5] whereby Hess's law is utilized for all calculated reactions. [5]

The reduction in process times or the amounts of charged materials are one of the main topics of dynamic converter modelling. Parameter studies could be done with the BOF model used since alterations in component parameters of the oxidation-reduction reactions, e.g. concentration or activity coefficients, influence the whole system. The backgrounds for this are thermodynamic and kinetic principles as well as the equation of the oxygen balance. The entire system of equations has to take in to account the following assumptions:

- chemical reactions on the interfacial surface are expeditious and equilibrated at each time step

- a limitation of reaction rates is based on mass transfer kinetics in the metal and slag phases
- lime concentration in the slag phase is equal at the interfacial surface and the slag bulk composition
- iron concentration in the metal phase is equal at the interfacial surface and the liquid metal bulk. [5]

Explanations of kinetic and thermodynamic calculations, the model flowsheet as well as the description of melting behaviour of slag formers, pellets and FeSi were published by Y. Lytvynuk et al. [5, 17]

## 2 MECHANISMS OF SCRAP MELTING IN THE BOF MODEL

Scrap is charged into the BOF at the beginning of the process. For simplification it is assumed in the BOF model used that the surface temperature of the scrap is equal to the hot metal temperature. The scrap particle itself is heated up through thermal conduction. In scrap melting, two mechanisms have to be considered if scrap melting and dissolution are to be defined in a BOF. [1, 4, 18, 19]

In the final stage of the BOF process the melt temperature exceeds the melting point of the scrap. In this case, scrap melting is defined as forced or convective melting. The heat transfer coefficient will be much higher than the mass transfer coefficient. [19, 20] In the case of convective scrap melting, the temperature difference between hot metal and scrap acts as the driving force. The following equation (Equation 1) characterizes the forced scrap melting:

$$-\frac{\partial r}{\partial t} = h_{\text{met}} * \frac{T_{\text{HM}} - T_{\text{liq}}}{(L + (H(T_{\text{scrap}}) - H(T_{\text{liq}}))) * \rho_{\text{scrap}}} \quad (1)$$

The radius of the scrap particle is  $r$  in unit [m]. The heat transfer coefficient in the metal phase is  $h_{\text{met}}$  in [ $\text{W m}^{-2}\text{K}^{-1}$ ]. The density of the scrap is  $\rho_{\text{scrap}}$  in [ $\text{kg m}^{-3}$ ] and the latent heat of the scrap melting is  $L$  in [ $\text{J kg}^{-1}$ ].  $T_{\text{HM}}$  and  $T_{\text{liq}}$  are the temperatures of the metal phase and the liquidus temperature of the scrap in [K]. [5, 17]  $H(T_{\text{scrap}})$  is the specific enthalpy of scrap at the actual temperature of the scrap surface and  $H(T_{\text{liq}})$  is the specific enthalpy of the scrap melting point, both in [ $\text{J kg}^{-1}$ ]. [21]

If the actual metal phase temperature is below the melting temperature of the scrap, diffusive scrap melting takes place. In this case, the scrap melting is driven by the difference in carbon concentration in the metal phase and the scrap. A decisive factor is the mass transfer coefficient for diffusive scrap melting. According to the Fe-Fe<sub>3</sub>C diagram, low carbon scrap has a higher melting point than hot metal with around 4.5 wt.-% of carbon. For diffusive scrap melting, the model described uses Equation 2 from Chigwedu C. [3]

$$-\frac{\partial r}{\partial t} = k_{\text{met}} * \ln \left( \frac{(\%C_{\text{HM}} - \%C_{\text{liq}}) * \rho_{\text{liquid}}}{(\%C_{\text{liq}} - \%C_{\text{scrap}}) * \rho_{\text{scrap}}} + 1 \right) \quad (2)$$

In Equation 2,  $k_{\text{met}}$  is the mass transfer coefficient in the metal phase in [ $\text{m s}^{-1}$ ].  $C_{\text{scrap}}$  and  $C_{\text{HM}}$  are the carbon concentrations in the scrap and hot metal in [wt.-%].  $C_{\text{liq}}$  describes the carbon concentration on the liquidus line. The density of the liquid hot metal is  $\rho_{\text{liquid}}$  and of the scrap it is  $\rho_{\text{scrap}}$ , both in [ $\text{kg m}^{-3}$ ]. [3] The values for the liquidus lines are approximated using a database of Fe-Fe<sub>3</sub>C-Si-Mn diagrams. The phase diagrams are generated by the FactSage™ FSstel database. [5, 22]

Through bottom stirring and oxygen blowing, the specific mixing power is calculated, which provides the basis for the mass transfer coefficient in the metal phase. The equation is a function of the total mixing power combined with the bath depth and the

vessel geometry. [17] The heat transfer coefficient of the metal phase is approximated solely by a function of specific mixing power. [5, 19]

### 3 INPUT PARAMETERS

The influence of the size and surface area of scrap particles was investigated for the dynamic simulation of a BOF converter. The following chapter gives an overview of the input parameters.

Hot metal, scrap, solid BOF slag and sand are charged at the start of the process. During the entire process time, only lime is charged for simplification. For each calculation, the amount of blown oxygen is equal. The period of oxygen blowing is always 12.6 min. The chemical compositions of industrial materials were used as input materials. In Table 1, the initial composition, the charged mass and charging temperature of the hot metal and the scrap are listed. For all investigations, the charged mass of scrap and the hot metal are constant.

**Table 1:** Specification of the hot metal and scrap used

	Unit	Hot metal	Scrap
Carbon content	[wt.-%]	4.536	0.737
Silicon content	[wt.-%]	0.410	0.349
Manganese content	[wt.-%]	1.171	1.060
Phosphorus content	[wt.-%]	0.100	0.013
Iron content	[wt.-%]	Rest	Rest
Mass	[t]	53.60	15
Temperature	[°C]	1318	20

The chemistry of the initial slag as well as their compositions and the amounts of the charged solid converter slag, sand and the added lime are shown in Table 2.

**Table 2:** Selected chemistry of added slag, sand and lime

	Unit	Initial slag	Solid BOF slag	Sand	Lime
SiO <sub>2</sub> content	[wt.-%]	11.32		92.79	0.980
MnO content	[wt.-%]	11.93	2.960		
P <sub>2</sub> O <sub>5</sub> content	[wt.-%]	1.330			
FeO content	[wt.-%]	29.66			
CaO content	[wt.-%]	40.08	7.320		92.37
MgO content	[wt.-%]	4.380	4.580		3.080
CO <sub>2</sub> content	[wt.-%]				2.400
H <sub>2</sub> O content	[wt.-%]				0.170
Fe <sub>2</sub> O <sub>3</sub> content	[wt.-%]		67.88		
Fe content	[wt.-%]		11.09		
Amount of charged material	[t]	0.001	1.000	0.172	2.800

### 4 INVESTIGATED SCRAP DIMENSIONS

For the investigation of the melting and dissolution behaviour of scrap, a common rail steel grade was used. It is assumed that the volume of the scrap is a sphere. For the investigation the diameter is changed in a first step (simulation numbers 1-3). The simulated scrap sizes are listed in Table 3. A second investigation (numbers 4-6)

assumes that the scrap is a 0.3 m high cylinder with one dimensional heat flow from the shell surface into the inside of the cylinder. In this case the diameter was also changed for this study. The input parameters for the scrap diameters are listed in Table 3.

**Table 3:** Starting diameters of scrap used

Simulation number	[-]	1	2	3	4	5	6
Sphere diameter	[m]	0.1	0.06	0.14	-	-	-
Cylinder diameter	[m]	-	-	-	0.1	0.06	0.14

According to the sphericity ( $S_{ph}$ ) defined by Wadell [23] in 1935, the surface area of the scrap was changed in the simulation. The sphericity of a particle is defined as the ratio of the surface area of a sphere to the surface area of the particle, whereby the sphere has the same volume as the given particle. The sphericity is given in Equation 3. [23, 24]

$$S_{ph} = \frac{\pi^{1/3}(6V_p)^{2/3}}{A_p} \quad (3)$$

In Equation 3,  $V_p$  defines the volume in [m<sup>3</sup>] and  $A_p$  the surface area of the particle in [m<sup>2</sup>]. The sphericity ( $S_{ph}$ ) of a sphere is 1 [-]. Isoperimetric inequality according to Equation 3 proposes, that every particle that is not a sphere has a sphericity below 1. In the simulation the reaction surface of the scrap is inversely multiplied with the sphericity of different geometric figures that are pointed out in Table 4. The reaction surface influences further the energy ( $Q_{heating}$ ), used for heating up the scrap particle. Equation 4 illustrates the calculation for the energy used for the heating the scrap particle.

$$Q_{heating} = \frac{\overline{\lambda(T)}}{r} * (T_{HM} - T_{Scrap}) * (A_p * \frac{1}{S_{ph}} * N) dt \quad (4)$$

In Equation 4,  $\overline{\lambda(T)}$  defines the temperature dependent thermal conductivity of the scrap particle in [W m<sup>-1</sup>K<sup>-1</sup>], which is based on an interpolation of five temperatures over the particle radius. The radius of the particle is r in [m].  $T_{HM}$  is the actual temperature of the hot metal and  $T_{Scrap}$  is the actual temperature of the scrap particle core in [K]. N is the number of particles [-].

The ideal cone is defined by  $h = 2\sqrt{2r}$ , whereby h is the height and r is the radius in [m]. The plate is assumed to be a parallelepiped with the dimensions (8mm\*2mm\*0.5mm). The results will be compared in the following chapter and are benchmarked to the sphere from the first simulation. [23, 24]

**Table 4:** Sphericity of various common objects [23, 24]

Simulation number	7	8	9	10	11	1
Scrap figure	Tetrahedron	Cube	Octahedron	Ideal cone	Plate	Sphere
Sphericity [-]	0.671	0.806	0.846	0.794	0.46	1
						

## 5 RESULTS AND DISCUSSION

The scrap melting during the BOF process was modelled using the aforementioned parameters. The following graphs demonstrate the calculated influence of the different scrap sizes and the assumed geometries on the melting and dissolution behaviour of scrap as well as the final bath temperature. They also outline the changes in the final chemical melt composition. Between minutes 8 and 10, a kink occurs in all figures, resulting from the change between diffusive and forced scrap melting. At this point, the melt temperature exceeds the melting temperature of the scrap. Under real process conditions, a smooth transition between the two melting mechanisms will take place. In the model, it is assumed that the melting point of scrap is specific to the liquidus line, while under real conditions the melting takes place in the two-phase area between the solidus and liquidus lines.

### 5.1 Influence of the scrap size

In Figure 1 the melting behaviour of scrap, assumed as spheres with various diameters from Table 3, is shown. It depicts that the melting of the low dimension scrap, diameter 0.06 m, starts very quickly but between 0.8 minutes and minute 3 it is very slow due to slow decarburization. After minute 3 the dissolution and melting begins to accelerate. This is explainable through Figures 2 and 3; compared to the same charging mass, a low dimension scrap has a higher overall surface where energy is transported from the melt to the scrap. This leads to a high cooling effect at the beginning of the process, pointed out in Figure 3. The high cooling effect also causes an inhibition of decarburization in the first process minutes. As mentioned in Chapter 2, the driving force of diffusive melting is the carbon difference between scrap and hot metal. These factors cause a slow melting behaviour of low dimensional scrap.

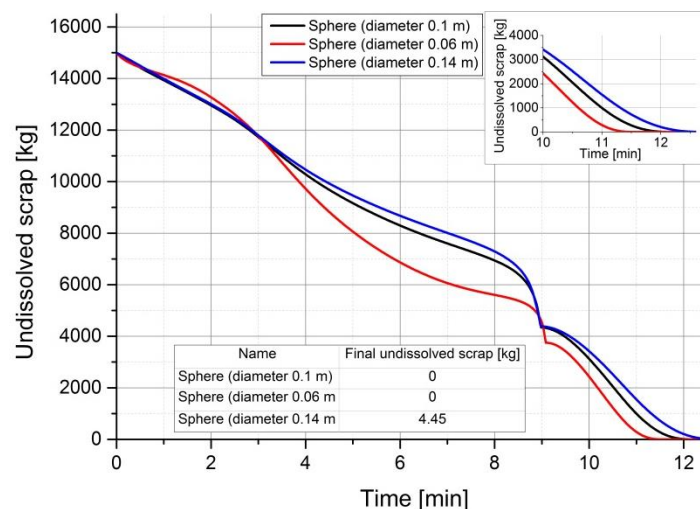


**Figure 1:** Melting and dissolution behaviour of spherical scrap particles.

Once the low dimensional scrap is heated up, the melting is faster than scrap with a higher diameter. Big scrap particles do not tend to melt completely until the constant blowing period, which is used in this simulation, has finished. However, the amount of undissolved scrap is very low, with 4.45 kg. The final values can be found in the table in all figures. In Figure 2 it is shown that the final temperature is lower in comparison to more voluminous scrap. The differences occur because of the open system. In

addition, spherical scrap with a diameter of 0.14 mm extracts less heat at the process start, illustrated in Figure 2.

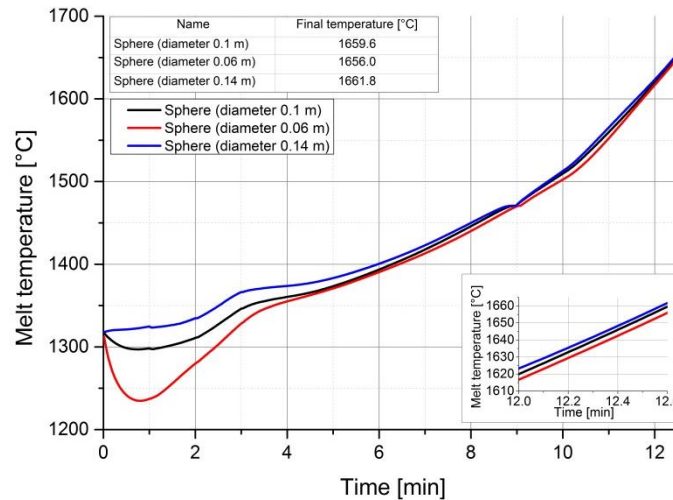


**Figure 2:** Melt temperature during the BOF process with spherical scrap.

According to the lower temperatures due to the greater surface, decarburization is slower if small scrap particles are used. Finally, the carbon content in the melt will be a little bit higher compared to the use of large scale scraps in a converter, as seen in Figure 3.

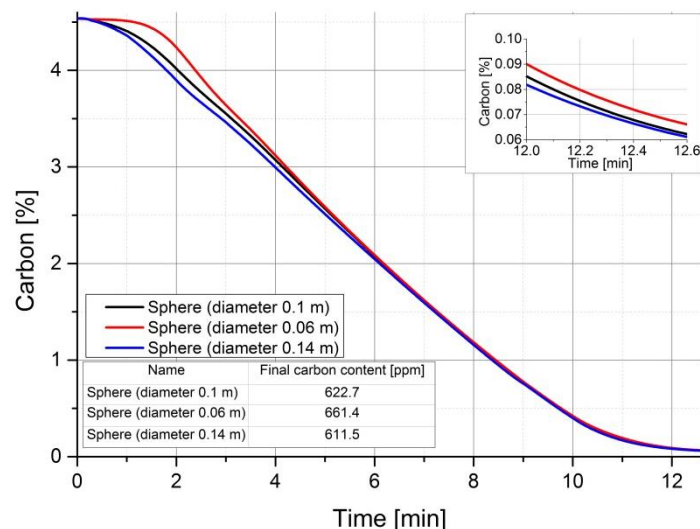


**Figure 3:** Carbon concentration of the liquid metal while spherical scrap is used.

The same behaviour of the scrap melting and dissolution could be seen if the scrap has a cylindrical geometry. As illustrated in Figure 4, a cylindrical scrap particle with a low diameter will melt faster than big scrap. Compared with the sphere, the green line in Figure 4, there seems to be no big difference in melting behaviour if the size is similar.

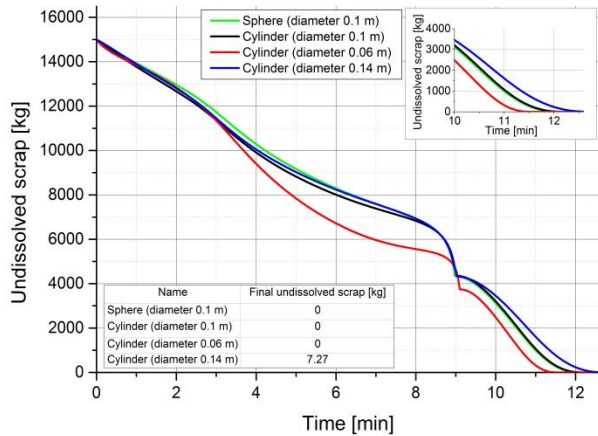


Figure 4: Melting and dissolution behaviour of cylindrical scrap particles.

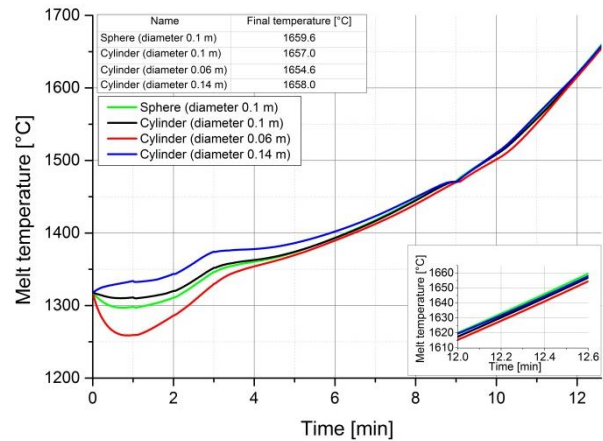


Figure 5: Melt temperature during the BOF process with cylindrical scrap.

The trajectories of the melt temperature show a similar behaviour if the scrap has spherical or cylindrical geometry, like it is pointed out in Figure 5. It could be seen that the strong decrease in the temperature due to the high overall scrap surface at the beginning of the blowing period will finally result in lower end temperatures after equal process times.

The compositions of manganese, phosphorus and silicon in the liquid metal are shown in Figure 6. The silicon content of the hot metal proceeds nearly unchanged. Only during the time range between 1 and 4 minutes does a lower content with higher scrap particle radius appear. The influence of the temperature can be seen in the graphs of manganese and phosphorus. A bigger radius of the scrap particles results in a higher temperature of the melt. This occurs as a result of the lower surface area compared to smaller lime particles, which means lower heat consumption from the scrap and more heat for the melt. The phosphorus oxidation needs a low temperature, which explains the earlier ascent of the phosphorus buckle if large-scale scrap is charged. With small scrap particles the melt temperature needs more time to reach the transition.

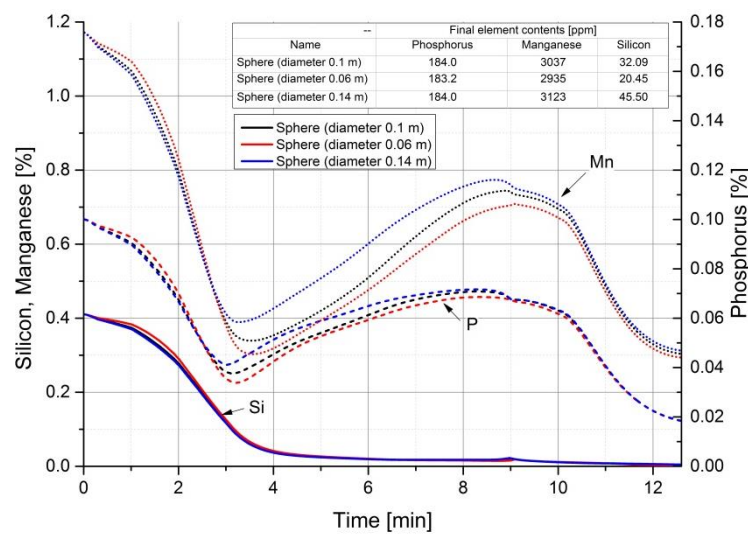
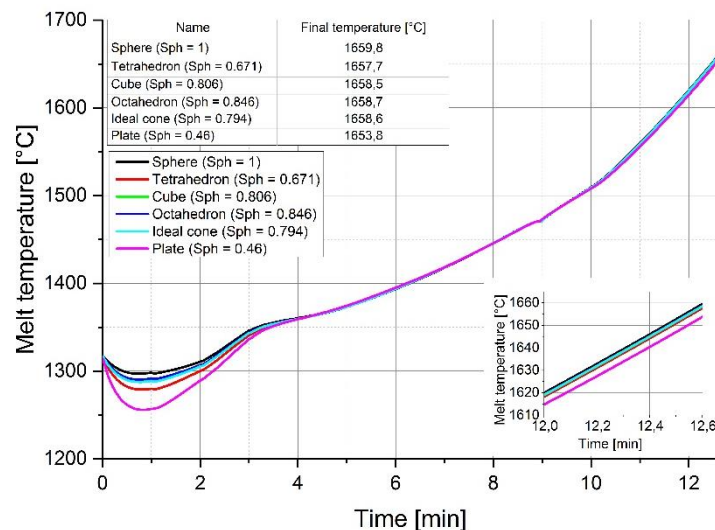


Figure 6: Influence of scrap size on metal behaviour.

## 5.2 Influence of the sphericity

Using sphericity (Sph) listed in Table 4, the surface of the scrap particle where heat transfer occurs was approximated. Because Sph is calculated with objects equal in volume, a sphere has the lowest surface of all analysed objects. This means the surface of a cylinder, plate or other geometrical bodies is larger. Figure 7 illustrates that the temperature will drop faster at the beginning of the process if the Sph is low, also resulting in a slightly lower final temperature.



**Figure 7:** Melt temperature during the BOF process with different sphericities for scrap particles.

Compared to the size change of the particles in Chapter 5.1, in this simulation the volume of a particle stays the same, which means the overall number of particles is also the same. Only the heat exchange surface is influenced by the sphericity. As shown in Figure 8, the lower the Sph, the lower the melting rate of the particle. This seems to be in conflict with Chapter 5.1 where small-sized scrap melts faster. But in the case of sphericity, the number of particles was not changed, so the overall surface of all particles was much higher for a longer period.

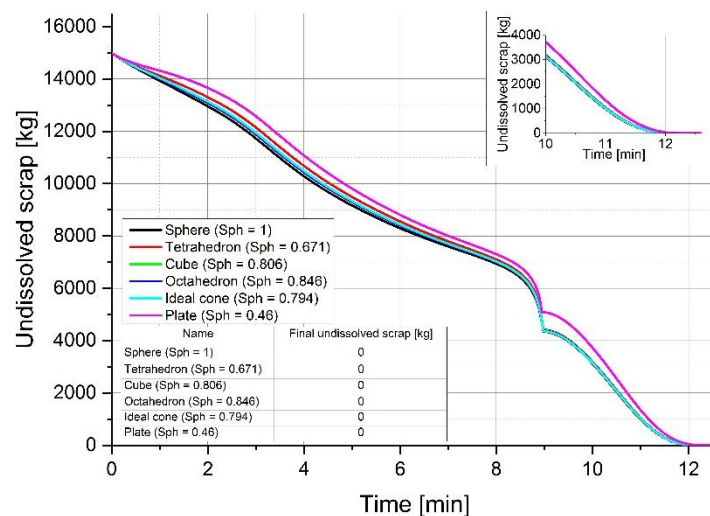


**Figure 8:** Melting and dissolution behaviour of scrap with various sphericities.

While a change in the size of a particle has a strong influence on the behaviour of manganese and phosphorus, the use of sphericities between 0.46 and 1 will show hardly any impact, as illustrated in Figure 9.

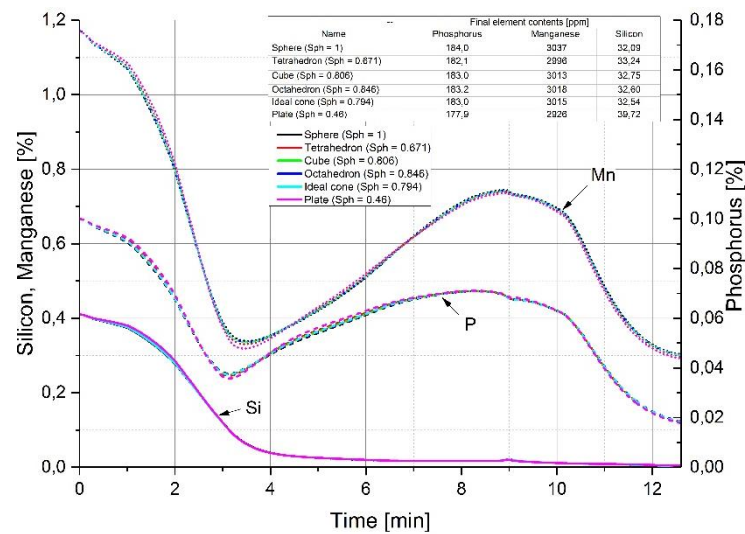


Figure 9: Influence of the sphericity on the metal behaviour.

As illustrated in Figure 10, the implementation has no effect on the mass balance of the final iron content in the slag and the melt. The manipulation of the temperature through the utilization of sphericity will change the course of the trajectories of the total amount of FeO in the slag and the melting behaviour of scrap, which results in the same total metal mass.

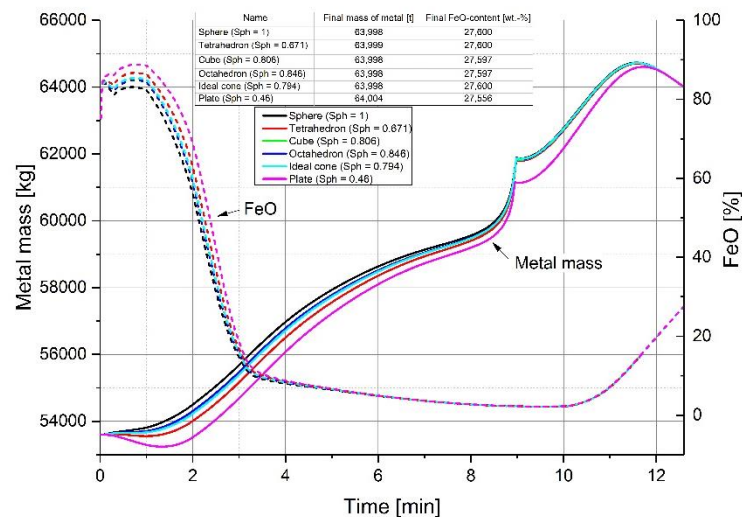


Figure 10: Influence of the sphericity on the mass balance of iron.

## 6 CONCLUSIONS

This paper points out the dissolution and melting behaviour of scrap using a dynamic BOF simulation based on complex chemical and physical phenomena. The BOF model is coded in MatLab® and also describes the behaviour of the metal and slag phases during the blowing period of the BOF process using thermodynamic and kinetic equations.

The aim of this study was to clarify the effect of the scrap size and geometry on the melting and dissolution behaviour of scrap as well as the influence on the final crude steel composition and temperature. First of all, it was shown that the scrap size plays a dominant role in the melting behaviour. If the scrap has a low diameter (0.06 m), the cooling effect decreases the hot metal temperature by more than 50 °C at the beginning of the process. This behaviour acts on the final temperature, which will be slightly lower if small-scale scrap is used. Attributable to this fact, the phosphorus and manganese composition is influenced by the lower temperatures. A second simulation, where scrap is assumed to be a cylindrical object, exhibits the same behaviour. If the scrap surface is manipulated with the form factor sphericity, the melting behaviour of scrap looks different, while the melt temperature shows the same conduct. The usage of sphericity for describing scrap melting in the BOF is easy to implement and gives a first estimation of the melting behaviour of scrap for the energy balance.

To sum up, the obvious reported in this paper clearly indicate that the size of scrap particles influences the melting and dissolution behaviour of the scrap. A sphericity between 0.46 (plate) and 1 (sphere) will only manipulate the trajectories during the BOF process and has hardly any influence on the final temperature or the chemical composition. The sphericity gives a first estimation to explain the scrap melting and dissolution behaviour but for a more exact description, the geometry of the scrap particles should be simulated with a two or three-dimensional model.

## Acknowledgments

The authors gratefully acknowledge the funding support of K1-MET GmbH, metallurgical competence center. The research programme of the K1-MET competence center is supported by COMET (Competence Centre for Excellent Technologies), the Austrian programme for competence centres. COMET is funded by the Federal Ministry for Transport, Innovation and Technology, the Federal Ministry for Science, Research and Economy, the provinces of Upper Austria, Tyrol and Styria as well as the Styrian Business Promotion Agency (SFG).

## REFERENCES

- 1 Turkdogan ET. Fundamentals of Steelmaking. London: The Institute of Materials; 1996.
- 2 Ghosh A and Chatterjee A. Ironmaking and Steelmaking theory and practice. Dehli: PHI Learning Private Limited; 2015.
- 3 Chigwedu C. Beitrag zur Modellierung des LD-Sauerstoffaufblasverfahrens zur Stahlerzeugung [Dissertation]. Clausthal: Technische Universität Clausthal; 1997.
- 4 Penz F, Bundschuh P, Schenk J, Panhofer H, Pastucha K, Paul A. Effect of Scrap Composition on the Thermodynamics of Kinetic Modelling of BOF Converter. Proceedings of 2<sup>nd</sup> VDEh-ISIJ-JK Symposium; Stockholm, Sweden 2017.
- 5 Lytvynyuk Y, Schenk J, Hiebler M, Sormann A. Thermodynamic and Kinetic Model of the Converter Steelmaking Process. Part 1: The Description of the BOF Model. Steel Research int. 2014; Vol. 85, No. 4, p. 537 – 543.
- 6 Hirai M, Tsujino R, Mukai T, Harada T, Masanao O. Mechanism of Post Combustion in the Converter. Transactions ISIJ 1987; Vol. 27, p. 805 – 813.
- 7 Bundschuh P, Schenk J, Hiebler M, Panhofer H, Sormann A. Influence of CaO Dissolution on the Kinetics of Metallurgical Reactions in BOF-process. Proceedings of the 7th European Oxygen Steelmaking Conference; Trinec, Czech Republic 2014.
- 8 Boychenko B, Okhotskiy V, Kharlashin P. The Converter Steelmaking. Dnipropetrovsk: Dnipro-VAL; 2006.

- 9 Ohguchi S, Robertson D, Deo B, Grieveson P, Jeffes J. Simultaneous dephosphorization and desulphurization of molten pig iron. *Iron and Steelmaking* 1984; Vol.11, No. 4, p. 202 – 213.
- 10 Kitamura S, Kitamura T, Shibata K, Mizukami Y, Mukawa S, Nakagawa J. Effect of stirring energy, temperature and flux composition on hot metal dephosphorization kinetics. *ISIJ International* 1991; Vol. 31, No. 11, p 1322 – 1328.
- 11 Kitamura S, Kitamura T, Aida T, Sakomura E, Koneko R, Nuibe T. Development of analysis and control method for hot metal dephosphorization process by computer simulation, *ISIJ International* 1991; Vol. 31, No. 11, p 1329 – 1335.
- 12 Kitamura S, Shibata H, Maruoka N. Kinetic Model of Hot Metal Dephosphorization by Liquid and Solid Coexisting Slags. *Steel Research Int.* 2008; Vol. 79, No. 9, p. 586 – 590.
- 13 Pahlevani F, Kitamura S, Shibata H, Maruoka N. Kinetic Model Dephosphorization in Converter. *Proceedings of SteelSim; Leoben, Austria* 2009.
- 14 Mukawa S, Mizukami Y. Effect of stirring energy and rate of oxygen supply on the rate of hot metal dephosphorization. *ISIJ International* 1995; Vol. 35, No.11, p 1374 – 1380.
- 15 Ishikawa M. Analysis of hot metal desiliconization behaviour in converter experiments by coupled reaction model. *ISIJ International* 2004; Vol. 44, No.2, p 316 – 325.
- 16 Higuchi Y, Tago Y, Takatani K, Fukagawa S. Effect of stirring and slag condition on reoxidation of molten steel. *ISIJ* 1998; Vol. 84, No.5, p 13 – 18.
- 17 Lytvyniyuk Y, Schenk J, Hiebler M, Mizelli H. Thermodynamic and kinetic modelling of the devanadization process in the steelmaking converter. *Proceedings of 6<sup>th</sup> European Oxygen Steelmaking Conference; Stockholm, Sweden* 2011.
- 18 Medhibozhskiy M. *Thermodynamic and Kinetic Fundamentals of Steelmaking*. Kyiv: Vischashkola; 1979.
- 19 Isobe K, Maede H, Ozawa K, Umezawa K, Saito C. Analysis of the Scrap Melting Rate in High Carbon Molten Iron. *ISIJ* 1990; Vol. 76, No.11, p 2033 – 2040.
- 20 Zhang L, Oeters F. *Schmelzen und Mischen von Legierungsstoffen in Stahlschmelzen*. Düsseldorf: Verlag Stahleisen GmbH; 2012.
- 21 Bundschuh P. *Thermodynamische und kinetische Modellierung von LD-Konvertern [Dissertation]*. Leoben: Montanuniversitaet Leoben; 2017.
- 22 Zarl M. *Development and evaluation of a BOF pre-processor model [Master Thesis]*. Leoben: Montanuniversitaet Leoben; 2017.
- 23 Wadell H. Volume, shape, and roundness of quartz particles. *Journal of Geology* 1935; Vol. 43, No. 3, p 250 – 280.
- 24 Penz F. *Charakterisierung des Hochofeneinsatzstoffes Sinter, mittels optischer 3D-Partikelanalyse [Bachelor thesis]*. Leoben: Montanuniversitaet Leoben; 2014.